TeleImpedance: Exploring the Role of Common-Mode and Configuration-Dependant Stiffness

A. Ajoudani, M. Gabiccini, N. Tsagarakis, A. Albu-Schäffer, and A. Bicchi

Abstract— **Humans explore and adapt neuro-motor strategies to cope with limitations of multi-joint impedance regulation mechanism. For instance, predictive control of degrees of redundancy further regulates the endpoint impedance in addition to co-contractions. Inspired by these observations, this paper proposes a novel Tele-Impedance algorithm that replicates the human's arm endpoint stiffness in robot by controlling the common-mode and configuration-dependant stiffness. Design of the controller and its stability is addressed and experimentally evaluated in robotic peg-in-hole task. Results of the proposed method are compared to the ones derived from Tele-Impedance implemented using classical Cartesian stiffness control. The interaction performance achieved highlights the possibility of adopting common mode stiffness in robots with adequate degrees of redundancy, in order to realize the desired task space impedance.**

I. INTRODUCTION

Humans demonstrate versatile and stable interactions with uncertain environments, exploiting learnt motor skills. Incorporation of such skills in modulation of mechanical properties of the human arm provides the possibility to confront environmental displacements by generating efficient and task-related restoring forces [1]. Modulation of such elastic forces is accomplished by adjustment of the stiffness properties of the muscles acting on the joints. Qualitative representation of the human endpoint stability in a certain posture is performed by the stiffness ellipsoid [2]. It has been observed that the size of the endpoint ellipsoid can be modulated by co-activation of agonist-antagonist muscles. However its orientation is severely constrained [3]. These observations imply that humans do not have voluntary and independent control over stiffness profiles of the arm joints. As a result, human arm endpoint will be less stiff in certain directions than others. In order to compensate for this inefficiency, self-selected postures further regulate the direction of the endpoint ellipsoid to meet task requirements. Indeed, contribution of the predictive postural control to mechanical stability in humans is shown to be more effective than the role of co-contraction [4], [5]. However, postural adjustments are extremely limited by the task constraints and mainly rely on the kinematic redundancy.

Replication of human-like impedance regulation mechanisms in robots can permit them to safely and efficiently operate in unstructured environments under unpredicted interaction scenarios. Traditionally, the implementation of impedance regulation in robots is achieved by introduction of torque controlled robots which can regulate actively their stiffness or full impedance properties by active control techniques [6]. More recently, developments of actuation systems which inherently integrate physical principles such as variable stiffness and damping [7], [8], [9], [10] permitted the intrinsic regulation of the robot impedance. Other studies explored the kinematic redundancy to regulate the endpoint stiffness profile. In the work of [11], based on a desired endpoint stiffness matrix, the joint stiffness levels were optimized and kept fixed. Consequently, a nullspace optimization algorithm (in less realtime planning layer) was adopted to additionally reduce the endpoint stiffness error. The minimum number of kinematic degrees of redundancy in order to replicate the desired full stiffness matrix was deeply discussed.

However, the impressive interaction skills of humans, in spite of the limited abilities of voluntary and independent control of joint stiffness profiles, propounds an insight for minimum kinematic and dynamic requirements in favor of robot's controller design. Towards this aim, one might be inspired by the neuro-motor policies for joint and endpoint stiffness modifications. For instance, concerning human arm postural stability, stiffness changes over shoulder and elbow joints are correlated [3], [12]. This observation provides the idea of adopting a *common mode stiffness* (CMS) across the joints and combine it with control of *configuration dependant stiffness* (CDS) to realize the desired endpoint stiffness. Larger number of degrees of kinematic redundancy (depending on the robot kinematics and task constraints), can lead to more accurate replication of the desired endpoint stiffness.

Inspired by above observations, in this paper we investigate the efficiency of a CMS-CDS controller in a robotic peg-in-hole task. The Human's task-related stiffness profile in addition to Cartesian position/orientation trajectories are replicated in the slave robot, using Tele-Impedance control [13]. Tele-Impedance as an alternative method to unilateral position based control or bilateral force reflecting control was previously proposed during teleoperated tasks which require significant dynamics variation or being performed in uncertain remote environments. The algorithm provides the robot with task-related stiffness profile in addition to position-

A. Ajoudani and A. Bicchi are with Interdepartmental Research Centre "E. Piaggio", Faculty of Engineering, University of Pisa, and with the Dept. of Advanced Robotics, Istituto Italiano di Tecnologia, Via Morego 30, 16163, Genova, Italy (e-mails: arash.ajoudani@iit.it and bicchi@centropiaggio.unipi.it).

N. G. Tsagarakis is with the Dept. of Advanced Robotics, Istituto Italiano di Tecnologia, Via Morego 30, 16163, Genova, Italy (e-mail: nikos.tsagarakis@iit.it).

M. Gabiccini is with the Department of Mechanical, Nuclear and Production Engineering, University of Pisa (e-mail: m.gabiccini@ing.unipi.it).

A. Albu-Schäffer is with the Institute of Robotics and Mechatronics, German Aerospace Center (DLR), Wessling, Germany (e-mail: Alin.Albu-Schaeffer@dlr.de).

orientation trajectories. The initial Tele-Impedance control [13], exploited traditional Cartesian stiffness control in order to realize the desired endpoint stiffness. Instead, in this paper, a novel human inspired real-time CMS-CDS controller is designed and implemented. The algorithm simultaneously regulates the CMS and CDS based on the error between time-varying desired stiffness matrix and the realized one at the robot endpoint. The results of the implementation of the CMS-CDS controller are experimentally evaluated in a peg in the hole task and compared to those derived from implementation based on the active cartesian control of the endpoint stiffness matrix.

The paper is structured as follows; section II presents the estimation of human arm impedance in 3D space and the identification-calibration process. Section III presents the design of the CMS and CDS controller. The experimental setup and results of the robotic peg-in-hole task by means of Tele-Impedance implemented using the proposed CMS-CDS controller and Cartesian impedance control are introduced in section IV and V respectively. Finally section VI addresses the conclusions.

II. Human Arm Impedance Modeling in 3D

Quantitative analysis of the mechanical properties of the human arm, when it comes to a contact with environment is commonly performed by means of imposing known displacements and probing the resulting steady state force response [2], [1]. However, the accurate and reliable application of perturbation in impedance estimation can be problematic when real-time estimation of the human arm impedance is required, especially during execution of constrained tasks. As a consequence, our previous studies were devoted to realize task-oriented profiles of the endpoint arm stiffness and force by means of corresponding patterns of activations in the involved muscles [13].

In our model, based on the fact that agonist-antagonist muscle co-contractions affect and modify the overall stiffness and viscous profiles of the arm endpoint and the linear dependency of force/stiffness to muscular activation/coactivations [14], [15], the overall mapping between muscular activities and resulting arm endpoint force (T_F) and stiffness (T_σ) in Cartesian coordination and around equilibrium position (close to isometric condition) is described by

$$\begin{bmatrix} F \\ \sigma \end{bmatrix} = \begin{bmatrix} T_F \\ T_\sigma \end{bmatrix} P + \begin{bmatrix} 0 \\ \sigma_0 \end{bmatrix}, \tag{1}$$

where $F, \sigma \in \mathbb{R}^3$ are the endpoint force and stiffness vectors, respectively, σ_0 is the intrinsic stiffness in relaxed conditions, and $P \in \mathbb{R}^n$ is the vector of muscular activities of the n considered muscles, as obtained from preprocessing EMG signals from electrodes applied on each muscle.

The end-point impedance can be modeled by three components, depending on posture, force, and co-contraction. While the first two components may be large and even dominating [5] in a large enough range of variations, literature also reports the existence and independence of co-contraction contribution to stiffness. Consequently, we consider a decomposition of the vector of muscular activations P in a force–generating component P_F and a stiffness–regulating component P_k. For the first-order linearized model (1), we write

$$P = T_F^R T_F P + \left(I - T_F^R T_F\right) P \stackrel{def}{=} P_F + P_k$$

where T_F^R denotes a right-inverse of T_F, i.e. a $n \times 3$ matrix such that $T_F T_F^R = I$, the 3×3 identity. The stiffness-generating component P_k is a projection of the measured EMG vector P in the kernel of the force-generating map T_F. An alternative description of P_k can be given as follows. Let N_F denote a basis matrix for the kernel of T_F, and let $\lambda = N_F^+ P_k = QP$ be the coordinates in that basis of P_k, where $Q \stackrel{def}{=} N_F^+ \left(I - T_F^R T_F\right)$. Using this model of stiffness regulation, we write

$$\sigma - \sigma_0 = M_\sigma Q P \tag{2}$$

where M_σ denotes the mapping from the kernel of T_F to stiffness variations. The map M_σ needs to be identified and calibrated once, based on direct measurements of human arm end point stiffness, at different coactivation levels as described in [13].

Inadequacy of this model for 3D stiffness estimation in whole human arm workspace (far from the reference posture) is the main disadvantage of proposed algorithm. Furthermore, force-related stiffness component of the model must be considered in tasks where large forces are realized at the contact point of the human arm. However, as far as the tasks to be performed by the master arm remain in a vicinity of the static posture in which the parameters are estimated, and the human arm is not applying external forces, the approach provides a reasonable approximation of the endpoint stiffness profile in real time.

Stiffness Model Calibration-Identification: One healthy subject (male; age 27) participated in the identification-calibration experiments. The subject stood upright with the feet side–by–side in front of a robotic arm. The robot arm was equipped at the endpoint with a handle connected to a 6–axis force and torque (F/T) sensor (ATI Mini-45). A passive spherical joint was used to connect the center of the handle to the F/T sensor to prevent the exertion of torques by the subject (see fig. 1). Displacements of the human arm at its endpoint (considered as the wrist center) were tracked by an Optitrack system (Natural Point, Inc.), with a nominal resolution of 0.02 mm. Optical markers were also placed at the shoulder and elbow of the subject's arm. Both force and position measurements were acquired at a sampling frequency of 200 Hz, and filtered by a low-pass Butterworth filter with cutoff frequency 15 Hz to eliminate noise.

Eight dominant muscles acting on elbow and shoulder joints (see Table I) were chosen as the sources of surface electromyograms (EMGs) recordings. The analogue EMG signals were measured and amplified with a Delsys-Bagnoli 16 (Delsys Inc.) apparatus. The acquired signals were band-pass filtered in the frequency range $[20, 450]$ Hz. The resulting

EMG signals were subsequently sampled at 2 kHz (PCI-6220, National Instruments) and full rectified for further processing. A digital non-causal FIR linear phase low-pass filter was used for the detection of the envelope of the signal, which approximately corresponds to muscle activity.

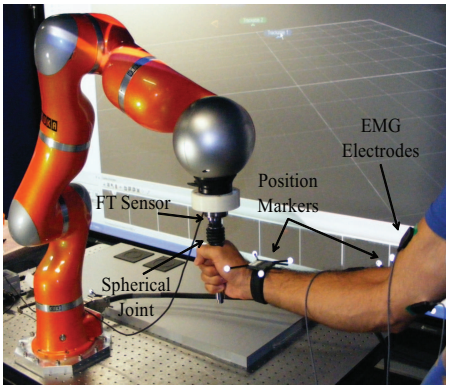

Fig. 1: Experimental setup used for the calibration experiments. Calibration consists of force regulation and perturbation experiments.

TABLE I: Muscles used for EMG measurements

Flexors		Extensors	
Monoarticular	Biarticular	Monoarticular	Biarticular
Deltoid clavicular part (DELC)	Biceps long head (BILH)	Deltoid scapular part (DELS)	Triceps long head (TRIO)
Pectoralis major clavicular part (PMJC)		Triceps lateral head (TRIA)	
Brachioradialis (BRAD)		Triceps medial head (TRIM)	

The robotic arm used is a seven degrees-of-freedom (DoF) KUKA LWR with DLR's Fast Research (FR) Interface [16]. The data acquisition and synchronization interface between the KUKA controller, the EMG acquisition board, the Optitrack position streaming data, the six axes F/T sensor were developed in C++.

The subject performed two identification experiments. Initially, the force–generating map T_F, was estimated and a basis of its nullspace and the projector matrix Q used in (2) were computed (see [13] for details). In a second set of experiments, aimed at estimating the stiffness–regulating map M_σ, we applied continuous stochastic perturbations to the subject's hand through the KUKA LWR handle in x, y and z directions in order to minimize voluntary stiffening behavior of the subjects arm [3]. The amplitude of the applied perturbations had the peak-to-peak value of 20 millimeters in each direction. Frequency spectrum of the perturbations were flat while decaying at the rate of 40 dB/Hz in frequencies higher than 4 Hz. This perturbation profile and corresponding forces in response, ensure adequacy of data for the identification of endpoint dynamics. Perturbations were applied at different co-contraction levels of the human arm. A rough stiffness indicator was graphically shown consisting of a bar of length proportional to the norm $|P|$ of the vector of muscle activations. Four different stiffness reference levels were provided in different trials.

The estimation of the endpoint stiffness in different trials was performed based on the measurement of corresponding pairs of forces and positions at the subject's wrist, following standard methods (see e.g. [3]). For this reason, multiple–input, multiple–output (MIMO) dynamics of the endpoint impedance was decomposed into the linear subsystems associating each input to each output. Based on this assumption, and indicating with $F_x(f)$, $F_y(f)$ and $F_z(f)$ the Fourier transforms of the endpoint force along the axes of the cartesian reference frame, with $x(f)$, $y(f)$ and $z(f)$ the transforms of the human endpoint displacements, the dynamic relation between the displacements and force variations can be described by

$$\begin{bmatrix} F_x(f) \\ F_y(f) \\ F_z(f) \end{bmatrix} = \begin{bmatrix} G_{xx}(f) & G_{xy}(f) & G_{xz}(f) \\ G_{yx}(f) & G_{yy}(f) & G_{yz}(f) \\ G_{zx}(f) & G_{zy}(f) & G_{zz}(f) \end{bmatrix} \begin{bmatrix} x(f) \\ y(f) \\ z(f) \end{bmatrix} \quad (3)$$

A non-parametric algorithm was adopted to identify the empirical transfer function of each of the SISO subsystems described above in frequency domain (MATLAB, The MathWorks Inc.). The smoothed spectral estimates of input and outputs (using windowing techniques) were fed to this algorithm in order to identify the each SISO transfer function. Consequently, we adopted a parametric, second order, linear model of each impedance transfer function of the type

$$G_{ij}(s) = I_{ij}\mathrm{s}^2 + B_{ij}\mathrm{s} + K_{ij}, \mathrm{s} = 2\pi f\sqrt{-1} \quad (4)$$

where I, B and K denote the endpoint inertia, viscosity and stiffness matrices, respectively. Multiple and partial coherence indexes were calculated. These indexes investigate the linear dependency of each output to all system inputs, and between single input and single output, respectively (Figure 2). Regarding strong linear dependency of the inputs and outputs in a certain frequency interval, the parameters of the second order linear model were identified based on least squares algorithm in frequency range from 0 to 10Hz.

Finally, in the postprocessing phase, experimental EMG vectors P were mapped in the EMG–to–force map nullspace through the previously computed projector matrix Q. The elements of the stiffness matrix K were used as estimates for the components of σ, and the map M_σ was estimated by applying a least–squared–error method to (2).

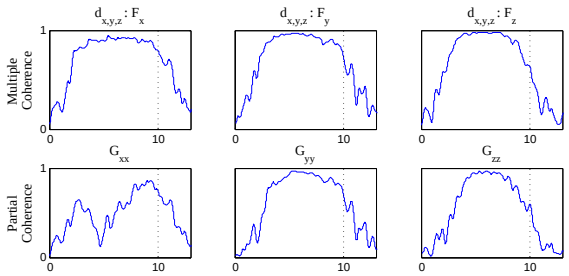

Fig. 2: Multiple and partial coherence values over frequency.

Figure(3) demonstrates the results of the non–parametric and second order model identification of the hand impedance transfer functions in the frequency range from 0 to 10Hz,

according to methods described above. The second order parametric impedance models presented (69.7%) of the data variance across all directions in minimum muscular activity trials in this frequency interval.

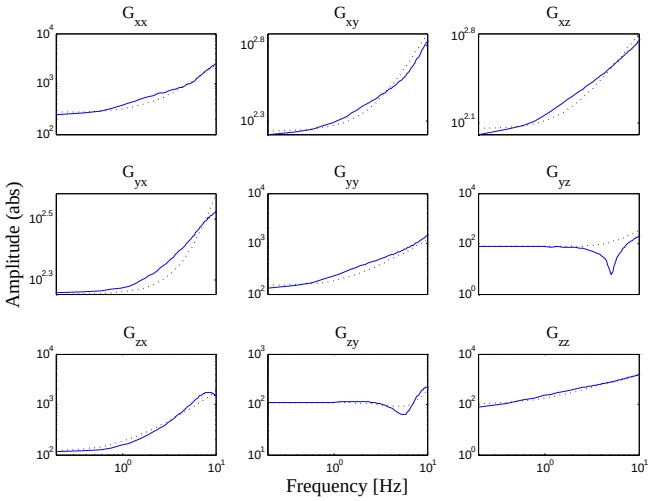

Fig. 3: Non–parametric (solid lines) and parametric second order (dotted lines) transfer functions of SISO impedance subsystems obtained from stochastic perturbations.

III. CONTROLLER DESIGN

In order to realize the human's desired endpoint stiffness profile at the slave's end effector, different strategies might be exploited. Cartesian impedance control [17] as a well-grooved technique, establishes a mass-spring-damper relationship between the Cartesian position and force. Implementation of such control scenario requires joint torque sensing and control. Recently the development of robotic systems equipped with passive variable stiffness actuation introduced a new design paradigm towards robots with intrinsic variable joint compliance properties. In these systems, to realize the full endpoint stiffness matrix the implementation of cross-joint stiffness must be taken into account in the robot design. An alternative solution can be provided by designing a hybrid controller which exploits passive and active control [18]. In order to further investigate this problem, in this paper, a human inspired control strategy is proposed.

Previous studies give evidence to common stiffness variations across human arm joints in static posture [3], [13] and as a result, stiffness ellipsoid angular changes will be severely limited. In such situation, secondary but dominant control strategy which exploits self-selected postures takes role and modifies the endpoint impedance profile to meet task needs [4]. Inspired by the superior interaction performance of the human arm achieved through the regulation of common mode stiffness and self-selected posture, we suggest and design a controller which regulates the common mode stiffness across the joints in addition to a nullspace controller which further minimizes the error between desired and realized endpoint stiffness.

Let K_c be the vector of common stiffness across the joints. Inspired by the correlation of stiffness changes in human arm joint as result of co-contractions, we consider a constant scaling factor across all joints as follows

$$K_s = J(q)^T K_h J(q) \tag{5}$$

where J denotes the manipulator Jacobian, q is the vector of joint angles and $K_h \in \mathbb{R}^{6\times 6}$ is the human endpoint stiffness. The diagonal matrix $K_s \in \mathbb{R}^{n\times n}$, with n number of joints in robot, will be calculated and normalized once and used for the rest of controller design. As a result $K_c = k_{cms} K_s$ where k_{cms} is optimized common mode stiffness in each time step. One may also consider optimization of constant joint scales (K_s) based on application and task needs.

In order to realize the desired endpoint stiffness matrix (K_h) provided by TeleImpedance algorithm, the following equation must be satisfied ideally

$$K_h \simeq (J^+)^T K_c J^+ \tag{6}$$

where J^+ denotes the pseudo-inverse, generally given by $J^+ = D^{-1}J^T(JD^{-1}J^T)^{-1}$ with D being a positive definite matrix. For the given problem we set $D = K_c$ as a metric tensor in the pseudo-inverse [11]. In this case if we take the time derivative of the equation (6), we will get

$$\begin{aligned}\dot{K}_h \simeq &[(J^+)^T K_s J^+ + (\dot{J^+})^T K_s J^+] k_{cms} \\ &+ [(J^+)^T K_s J^+]\dot{k}_{cms}\end{aligned} \tag{7}$$

where two terms in first bracket of equation (7) being each others transpose. Definition of derivative of the pseudo-inverse of jacobian in symbolic equation is problematic due to its complexity. However, based on a proven theorem [19], we can establish the derivative of pseudo-inverse of Jacobian matrix as follows

$$\begin{aligned}\frac{dJ^+}{dt} = &-J^+\frac{dJ}{dt}J^+ + J^+(J^+)^T\frac{dJ^T}{dt}N_J{}^{\perp} + \\ &{}_JN^{\perp}\frac{dJ^T}{dt}(J^+)^T J^+\end{aligned} \tag{8}$$

where $N_J{}^{\perp}$ and ${}_JN^{\perp}$ are the projectors on the orthogonal complement of the column and row space of J, respectively.

Equation (7) can be factorized with respect to $\dot{q}$. Therefore, by reshaping the equation in vector form through the operator vect$(\cdot)$ (the operator extracts the 21 independent elements of 6×6 symmetric matrix), we get

$$\begin{aligned}\text{vect}\{\dot{K}_h\} \simeq &\text{vect}\{k_{cms}[(J^+)^T K_s A_q + A_q^T K_s J^+]\}\dot{q} \\ &+ \text{vect}\{[(J^+)^T K_s J^+]\}\dot{k}_{cms}\end{aligned} \tag{9}$$

where $A_q = \frac{dJ}{dq}$. To simplify the expressions we can introduce $J_q \overset{def}{=} \text{vect}\{k_{cms}[(J^+)^T K_s A_q + A_q^T K_s J^+]\}$ and $J_k \overset{def}{=} \text{vect}\{[(J^+)^T K_s J^+]\}$. Therefore we can write

$$\dot{K}_h = J_q\dot{q} + J_k\dot{k}_{cms} \tag{10}$$

Now, if we take into account that $\dot{q}$ is allowed to vary in the nullspace of J, while complying with the prescribed motion of the end-effector, then we can write

$$\dot{q} = J^+ K_p e_p + N_J{}^{\perp}\dot{\lambda} \tag{11}$$

where K_p is the gain matrix for Cartesian position error e_p and $\dot{\lambda}$ a free parameter controlling the nullspace velocity component. Above expression is a classical inverse kinematics problem, based on the pseudo-inverse of the Jacobian. Now, combining equation (11) and (10) we get

$$\dot{K}_h = J_q(J^+ K_p e_p + N_J{}^{\perp}\dot{\lambda}) + J_k \dot{k}_{cms} \tag{12}$$

Defining $\dot{\tilde{K}}_h \stackrel{def}{=} \dot{K}_h - J_q J^+ [K_p e_p]$ and $J_\lambda \stackrel{def}{=} J_q N_J{}^{\perp}$, we can write

$$\dot{\tilde{K}}_h = \begin{bmatrix} J_\lambda & J_k \end{bmatrix} \begin{bmatrix} \dot{\lambda} \\ \dot{k}_{cms} \end{bmatrix} =: J_y \dot{y} \tag{13}$$

Above equation resembles the structure of inverse kinematics problem of defective robots, since we are dealing with the tracking of $\dot{\tilde{K}}_h \in \mathbb{R}^{21}$ by using k_{cms} and degrees of kinematic redundancy. Now, by defining the vectorial stiffness error $e_s = \text{vect}\{K_h - k_{cms}[(J^+)^T K_s J^+]\}$, we can set up classical update laws. Consequently, by exploiting the update law based on the pseudo-inverse of J_y we get

$$\dot{y} = J_y{}^+ \left[\dot{\tilde{K}}_h + K_{ps} e_s\right], \tag{14}$$

where K_{ps} is the gain associated to the stiffness error e_s.

Stability Analysis: To evaluate the convergence of the above algorithms, [1] we can introduce a Lyapunov candidate

$$V = \frac{1}{2} e_s^T K_{ps} e_s. \tag{15}$$

With positive definite and symmetric K_{ps}, the function will be positive definite in e_s. Time derivative of the function is

$$\dot{V} = e_s^T K_{ps} \dot{\tilde{K}}_h - e_s^T K_{ps} J_y \dot{y}. \tag{16}$$

By inserting the control law from Eq. (14), we obtain

$$\dot{V} = e_s^T K_{ps}(I - J_y J_y^+)\dot{\tilde{K}}_h - e_s^T K_{ps} J_y J_y^+ K_{ps} e_s. \tag{17}$$

In Eq. (17), we can easily recognize some interesting properties of the two terms. Since $J_y J_y^+$ is a projector onto the range space $\mathscr{R}(J_y)$ of J_y, it has the same column space as J_y, that is $\mathscr{R}(J_y J_y^+) = \mathscr{R}(J_y)$. In fact, a simple SVD decomposition of J_y in the form $J_y = USV^T$, with $U = [u_1\ u_2\ U_n]$, where u_1 and u_2 are the unit orthogonal vectors that form a basis for $\mathscr{R}(J_y)$, results in $J_y J_y^+ = u_1 u_1^T + u_2 u_2^T$. This also makes clear that there are two positive and unitary eigenvalues, corresponding to the eigenvectors u_1 and u_2, and the zero eigenvalue with multiplicity equal to $\dim(\mathscr{N}(J_y^T))$ along the orthogonal complement $\mathscr{N}(J_y^T) = \mathscr{R}(U_n)$.

This indicates that the second term is negative definite as long as $K_{ps} e_s \in \mathscr{R}(J_y)$, and it vanishes when $K_{ps} e_s \in \mathscr{N}(J_y^T)$. On the contrary, the projector $(I - J_y J_y^+)$ is such that the first term vanishes when $\dot{\tilde{K}}_h \in \mathscr{R}(J_y)$ (it is worth observing that $\mathscr{N}(I - J_y J_y^+) = \mathscr{R}(J_y)$), while being different from zero with unspecified sign otherwise. Therefore, we can conjecture that if the time dependent term $\dot{\tilde{K}}_h$ is dominated by the second term (in the cases when $K_{ps} e_s \notin \mathscr{N}(J_y^T)$), then $\dot{V} < 0$ and the local asymptotic tracking is guaranteed.

[1] concerning our experimental setup, we simplify the analysis to two degrees of redundancy. However, the analysis can be performed in general case. Alternative solution can be proposed by using Jacobian transpose instead of pseudo-inverse in eq. (14)

IV. PEG-IN-HOLE EXPERIMENTAL SETUP

Efficiency of proposed approach to cope with contact stability issues is evaluated in a Peg-in-Hole task, a classical benchmark for spatial planning with uncertainties. Comparative analysis of the proposed algorithm was performed considering interaction forces and the realized stiffness matrix error (e_s).

The experimental setup and information flow are shown in fig. 4. Body markers were attached to the wrist in order to provide the reference trajectory for robot motion. The robot base frame was considered as the overall reference frame for other frames (Optitrack and FT sensor). The position and orientation path of the human wrist was measured, low-pass filtered (cutoff 15Hz) and used for trajectory planning. Incremental joint position references were sent to the robot, derived from the position tracking errors in six dimensions (e_p). This approach was used to cope with drift and tracking inaccuracy due to possible delays between reference commands and generated movement in the slave end-effector. During the experiment, the operator was asked to move his/her hand to reach the reference configuration (where the stiffness model is calibrated), and finally to teleoperate the robot to insert the peg in the hole. The master could see the slave arm, including the peg and hole. No peg was hold by the master, nor did he receive any feedback except visual. It should be noted that in the reaching phase, where stiffness calibration is not accurate, there are no interactions with the environment.

The experiment consisted in two parts. In both parts, human's equilibrium positions, orientation and endpoint stiffness profiles as estimated by the TeleImpedance algorithm were sent to remote side. Damping values along x, y, and z, were set to a constant value of $D = [0.7, 0.7, 0.7]$ N.s/m. Further extensions of the TeleImpedance method, providing the possibility of reproducing the endpoint damping behavior of the human with the slave robot arm, are possible but have not been demonstrated yet.

In the first part, human's endpoint stiffness matrix is realized by classic Cartesian control [13], while, in the second part, the proposed CMS-CDS algorithm was in charge of realizing the desired stiffness in robot's end-effector. Indeed, in the second part, both CMS and CDS control inputs are simultaneously updated based on the error between master's time-varying endpoint stiffness profile and the realized one. All processing and control algorithms were performed in real-time. Software interfaces, sampling frequencies, and hardware specifications are all identical to those reported in the previous section.

V. EXPERIMENTAL RESULTS

The minimum required DoF in order to realize the desired full stiffness matrix (with 21 stiffness DoF) has bees addressed previously [11]. The larger the number of degrees of kinematic redundancy the more precise replication of desired endpoint stiffness can be accomplished. In our experiments, the KUKA robotic arm with 7 DoF is used. Since the peg-in-hole task with round peg required 5 DoF, the remaining 3

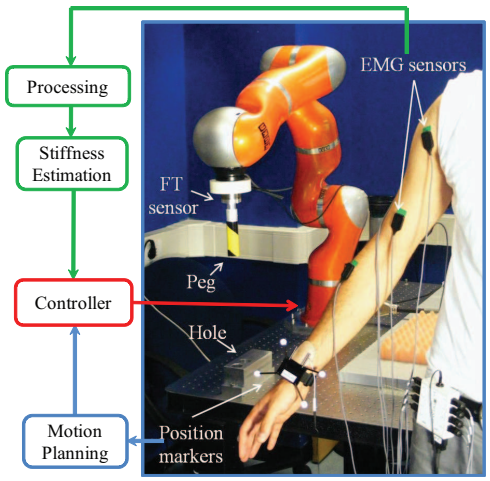

Fig. 4: Peg-in-Hole experimental setup. KUKA light weight robotic arm, EMG electrodes, peg, hole, position tracking markers and F/T sensor are shown.

DoF (CMS and two degrees of kinematic redundancy), are the ones used by the controller to realize K_h and explore the role of CMS and CDS regulations in minimization of e_s. Figure (5) demonstrates the effects of CDS controller while being added to CMS. In this experiment, the human's endpoint stiffness was estimated once, kept fixed and used during the whole experiment. As it is shown in the plots, the error decreases approximately 10%, once the overall controller (CDS-CMS) is applied. Figure 6, demonstrates the replicated

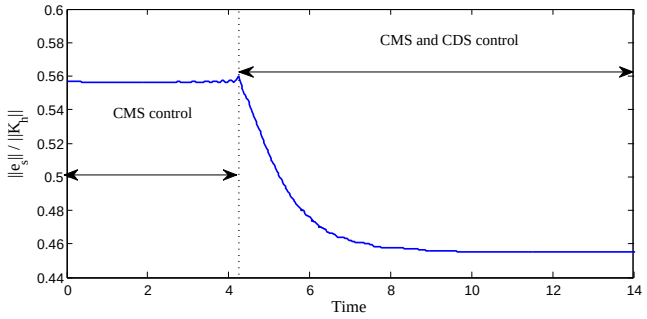

Fig. 5: Normalized error while the desired endpoint stiffness is fixed. At the beginning of experiment, only CMS is updated. Then at $t \simeq 4.2sec$, the CDS-CMS controller takes role.

endpoint stiffness ellipsoids of the same experiment, while exploiting the classical Cartesian stiffness (CSC), CMS-CDS and only CMS controllers. In this figure, stiffness ellipsoid in 3D is projected in three planes. As it is shown in the plots, while the CSC ellipsoids coincide with the desired ones, effective modifications of ellipsoid geometry is achieved by proposed CMS-CDS algorithm, even by holding small number of degrees of kinematic redundancy.

During the peg-in-hole experiments, the master moves his arm in the space and aligns the peg with the hole direction with the final posture of master's arm conforming to the reference posture. Consequently, the user modulates his endpoint stiffness by performing co-contractions. Figure (7) demonstrates the interaction forces between the peg, surface

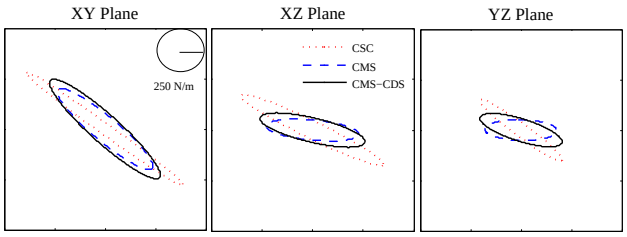

Fig. 6: Robot endpoint stiffness ellipsoids replicated by Tele-Impedance under Cartseian stiffness (CSC), CMS-CDS and CMS controllers. Cartesian stiffness ellipsoids coincide with the desired ones.

and the hole while Tele-Impedance control replicates the desired endpoint stiffness at the slave's end-effector under Cartesian stiffness (upper plot) and CMS-CDS (lower plot) controllers. It has been previously shown that while fixed and high stiffness values produce very high interaction forces, fixed-low stiffness values cannot overcome frictional forces between the peg and the hole [12]. For this reason, continuous modulation of endpoint stiffness is highly required concerning safety and performance.

As shown in the plots, similar interaction forces are resulted by Cartesian stiffness and CMD-CDS controllers during the insertion and pull-off phase. This implies that the endpoint stiffness profiles of both algorithms resemble, since they hold approximately the same path of equilibrium positions. However, while exploiting only CMS instead of overall CMS-CDS controller, the error sum ($\sum e_s$) increased around 25%. The adaptation of CMS, as result of co-contractions, during the peg-in-hole experiment is shown in fig. 8.

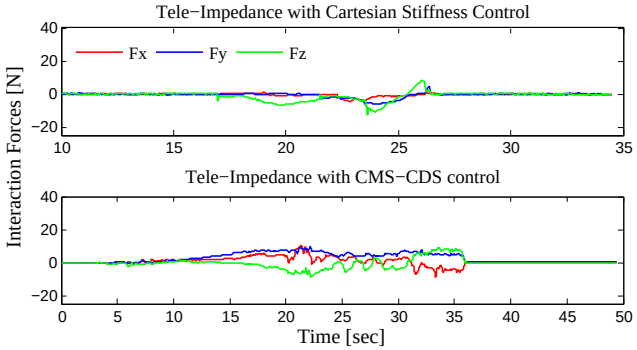

Fig. 7: Interaction forces for peg-in-hole experiments as result of Tele-Impedance algorithm with Cartesian stiffness control (upper plot) and CMS-CDS control (lower plot).

It is worth noting that inspired by observations in human arm impedance regulation mechanism, the purpose of this study was to explore the single stiffness synergy across the arm joints. However, one may consider increased number of controlled joint stiffness values (CMS) to possibly improve stiffness tracking performance. Eventually, our proposed CDS controller will be adopted to further reduce the error between the desired stiffness matrix and the one realized at the robot endpoint. Such scenario will provide the possibility

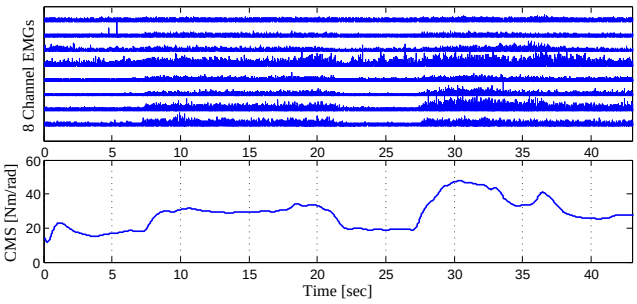

Fig. 8: Eight channel raw EMGs (upper plots) and adapted common mode stiffness (lower plot).

of design and control of robotic arms with $n+m$ actuators, with n and m being number of joints and stiffness synergies, respectively (where in this work $m=1$).

VI. CONCLUSIONS

Inspired by human's neuro-motor strategies for impedance control, this work introduced the novel concept of Tele-Impedance, while exploiting common mode and configuration dependant stiffness control. The initial Tele-Impedance algorithm [13] provides the robot with the task-related human impedance combined with the position/orientation trajectories. This reference command is being executed under classic Cartesian impedance control. However, in the novel proposed control methodology, the CMS and CDS are simultaneously adapting relying on the error between time-varying human's endpoint stiffness and the one, realized at robot's end-effector. The controller design and proof of convergence is discussed and experimentally evaluated in robotic peg-in-hole task.

Similar interaction performances accomplished by the proposed algorithm and the classic Cartesian impedance control based Tele-Impedance gives rise to the idea of control of single stiffness synergy in addition to the task-oriented degrees of kinematic redundancy, in order to accomplish the task. The same but more sophisticated performance is observed by human since they rely on many degrees of freedom not only concerning the arm, but the whole body. Furthermore, humans, if not constrained, move around the task and predictively choose the best posture to further regulate endpoint impedance. This fact additionally highlights the use of mobility in addition to the single stiffness synergy and other kinematic redundancy. We believe that the human-inspired modulation of the endpoint impedance during execution of tasks with significant dynamics variation inquiries can finally permit robots or assistive devices to reach high interaction performances, and also possibility of demonstrating a versatile and stable behavior even when interacting with environments with dynamic uncertainties.

VII. ACKNOWLEDGMENTS

This work is supported by the European Community, under grants FP7 ICT-287513 "SAPHARI" and under the ERC Advanced Grant no. 291166 "SoftHands" (A Theory of Soft Synergies for a New Generation of Artificial Hands).

REFERENCES

[1] E. Burdet, R. Osu, D. Franklin, T. E. Milner, and M. Kawato, "The central nervous system stabilizes unstable dynamics by learning optimal impedance," *Nature*, vol. 414, no. 6862, pp. 446–449, 2001.

[2] R. Osu and H. Gomi, "Multijoint muscle regulation mechanism examined by measured human arm stiffness and EMG signals," *Journal of Neurophysiology*, vol. 81, pp. 1458–1468, 1999.

[3] E. Perreault, R. Kirsch, and P. Crago, "Voluntary control of static endpoint stiffness during force regulation tasks," *Journal of Neurophysiology*, vol. 87, pp. 2808–2816, 2002.

[4] R. Trumbower, M. Krutky, B. Yang, and E. Perreault, "Use of self-selected postures to regulate multijoint stiffness during unconstrained tasks," *PLoS One*, vol. 4, no. 5, 2009.

[5] T. Milner, "Contribution of geometry and joint stiffness to mechanical stability of the human arm," *Experimental Brain Research*, vol. 143, pp. 515–519, 2002.

[6] R. Bischoff, J. Kurth, G. Schreiber, R. Koeppe, A. Albu-Schäffer, A. Beyer, O. Eiberger, S. Haddadin, A. Stemmer, G. Grunwald *et al.*, "The kuka-dlr lightweight robot arm-a new reference platform for robotics research and manufacturing," in *41st International Symposium on on Robotics (ROBOTIK)*. VDE, 2010, pp. 1–8.

[7] M. Laffranchi, N. Tsagarakis, F. Cannella, and D. Caldwell, "Antagonistic and series elastic actuators: a comparative analysis on the energy consumption," in *IEEE/RSJ International Conference on Intelligent Robots and Systems, 2009.* IEEE, 2009, pp. 5678–5684.

[8] A. Jafari, N. Tsagarakis, B. Vanderborght, and D. Caldwell, "A new variable stiffness actuator (CompAct-VSA): Design and modelling," in *IEEE/RSJ International Conference on Intelligent Robots and Systems (IROS)*, 2011, pp. 378–384.

[9] M. Mancini, G. Grioli, M. G. Catalano, M. Garabini, F. Bonomo, and A. Bicchi, "Passive impedance control of a qboid multi-dof vsa manipulator," in *International Conference of Robotics and Automation - ICRA 2012*, Saint Paul, MN, USA, May 14 - 18 2012.

[10] M. Grebenstein, A. Albu-Schaffer, T. Bahls, M. Chalon, O. Eiberger, W. Friedl, R. Gruber, S. Haddadin, U. Hagn, R. Haslinger *et al.*, "The dlr hand arm system," in *IEEE International Conference on Robotics and Automation (ICRA)*. IEEE, 2011, pp. 3175–3182.

[11] A. Albu-Schaffer, M. Fischer, G. Schreiber, F. Schoeppe, and G. Hirzinger, "Soft robotics: what cartesian stiffness can obtain with passively compliant, uncoupled joints?" in *IEEE/RSJ International Conference on Intelligent Robots and Systems, 2004.*, vol. 4. IEEE, 2004, pp. 3295–3301.

[12] A. Ajoudani, N. G. Tsagarakis, and A. Bicchi, "Tele-impedance: Preliminary results on measuring and replicating human arm impedance in tele operated robots," in *IEEE International Conference on Robotics and Biomimetics - ROBIO 2011*, 2011, pp. 216 – 223, youtube: http://www.youtube.com/watch?v=KPO6IO7Tr-Q.

[13] ——, "Tele-impedance: Towards transferring human impedance regulation skills to robots," in *International Conference of Robotics and Automation - ICRA 2012*, Saint Paul, MN, USA, May 14 - 18 2012.

[14] L. Selen, P. Beek, and J. V. Dieen, "Can co-activation reduce kinematic variability? a simulation study," *Biological Cybernetics*, vol. 93, pp. 373–381, 2005.

[15] D. Franklin, R. Osu, E. Burdet, M. Kawato, and T. Milner, "Adaptation to stable and unstable dynamics achieved by combined impedance control and inverse dynamics model," *Journal of Neurophysiology*, vol. 90, no. 5, pp. 3270–3282, 2003.

[16] G. Schreiber, A. Stemmer, and R. Bischoff, "The fast research interface for the kuka lightweight robot," in *IEEE Conference on Robotics and Automation (ICRA)*, 2010.

[17] A. Albu-Schaffer and G. Hirzinger, "Cartesian impedance control techniques for torque controlled light-weight robots," in *Robotics and Automation, 2002. Proceedings. ICRA'02. IEEE International Conference on*, vol. 1. IEEE, 2002, pp. 657–663.

[18] F. Petit and A. Albu-Schaffer, "Cartesian impedance control for a variable stiffness robot arm," in *IEEE/RSJ International Conference on Intelligent Robots and Systems (IROS)*. IEEE, 2011, pp. 4180–4186.

[19] G. Golub and V. Pereyra, "The differentiation of pseudo-inverses and nonlinear least squares problems whose variables separate," *SIAM Journal on numerical analysis*, pp. 413–432, 1973.